ARCHIVES of FOUNDRY ENGINEERING

Published quarterly as the organ of the Foundry Commission of the Polish Academy of Sciences

ISSN (1897-3310)
Volume 11
Special Issue
3/2011

171 – 176

31/3

Analysis by numerical calculations of the depth and dynamics of the penetration of ordered cellular structure made by casting from AlSi10Mg eutectic alloy

J. Piekło [a], S. Pysz [b], M. Małysza [b], A. Karwiński [b]*

[a] Faculty of Foundry Engineering, AGH University of Science and Technology,
Reymonta 23, 30-059 Krakow, Poland
[b] Foundry Research Institute
Zakopiańska 73, 30-418 Kraków, Poland
*Corresponding author. E-mail address: akarw@iod.krakow.pl

Received 22.07.2011 accepted in revised form 27.07.2011

Abstract

Owing to high plastic deformability while maintaining stress values constant and relatively low, ordered cellular structures are characterised by excellent properties and the ability to dissipate the impact energy. Due to the low weight, structures of this type can be used, among others, for different parts of motor vehicles. For tests, a trapezoidal ordered cellular structure of 50.8 x 50.8 x 25.4 (mm) overall dimensions was selected. It was made as an investment casting from AlSi9Mg eutectic alloy by the method of Rapid Prototyping (RP). During FEM computations using an Abaqus programme, it was assumed that the material is isotropic and exhibits the features of an elastic – plastic body, introducing to calculations the, listed in a table, values of the stress-strain curve obtained in tensile tests performed on a MTS testing machine (10T). The computations used Johnson - Cook model, which is usually sufficiently accurate when modelling the phenomena of penetration of an element by an object of high initial velocity. The performed numerical calculations allowed identification of changes in speed and energy of the penetrator during structure perforation.

Keywords: Cellular structures, Aluminium alloys, FEM simulation, Penetration of an element,

1. Introduction

Ordered cellular structures of a "sandwich" type are characterised by high plastic deformability while maintaining the stress values constant and relatively low, and, owing to this, have excellent properties dissipating the impact energy, which makes them suitable for energy absorbers in a number of constructions subjected to extreme conditions of loads and ballistic impacts with the internal structure remaining relatively intact [1], [2], [3].

The phenomenon of perforating the cast structure with a steel penetrator can be divided into four stages as in the case of a projectile penetrating an armour [4]:

- penetrator impact contact with the casting surface,
- penetrator entering the casting at a constant speed,
- penetrator movement inhibited by the forces of inertia and resistance offered by the alloy,
- crater formed finally after arresting the penetrator movement.

Because of high initial speeds of the penetrator (up to 720 m/s), considered in the examined numerical models based on the finite element method (FEM), the description of the occurring phenomena should allow for their dynamic nature and complexity of the, changing in time, conditions of contact between the penetrator surface and the casting. It is also necessary to use appropriate constitutive equations describing the investigated materials and the destruction model, considering also the thermal effects. Below the results of computer simulation of the phenomena under consideration supported with material studies and experiments are presented.

2. Numerical model of the phenomena

The construction of a numerical model reflecting the phenomena that accompany the casting perforation with a penetrator required the determination and adoption of assumptions regarding:

- the shape and dimensions of both the cast cellular structure and penetrator,
- constitutive equations for cast alloy and penetrator material,
- model of both materials decohesion,
- boundary and initial conditions,
- the conditions of contact phenomena,
- computation algorithm,
- the type of finite elements and the density of a FEM mesh.

Another issue was selection of the calculation results which should be saved for further studies of this type to enable a comparison of numerical models with each other, on the one hand, and of the behaviour of various alloys under the influence of dynamic loads, on the other. Below, the assumptions adopted will be discussed with particular emphasis put on issues concerning modelling of material properties and the decohesion mode.

2.1. Shape and dimensions of model components

For tests, trapezoidal ordered cellular structure of 50.8 x 50.8 x 25.4 (mm) overall dimensions (3D drawing made in SolidWorks) was selected. It was next made as an investment casting from eutectic Al - Si alloy using a Rapid Prototyping technique (RP). Details of design and construction of mould and cast model (Fig. 1) can be found in the author's article [5]. The penetrator was a φ 8 mm and 30 mm long cylinder sharp-pointed on the end which perforates the model structure.

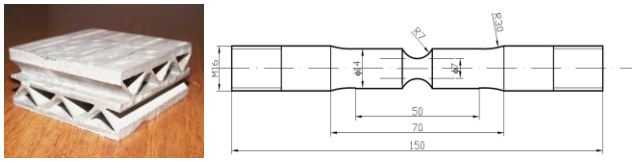

Fig. 1. Casting of a trapezoidal structure and specimen with annular notch of φ = 7 mm

2.2. Constitutive model of Al - Si alloy

The description of the behaviour of the cast alloy of the chemical composition as shown in Table 1 during the dynamic collision with a steel penetrator is very complex and requires introduction of the necessary simplifications; additionally, alternative models of plastic deformation can be adopted.

Table 1.
Percent content of elements in Al – Si alloy

Al	Si	Cu	Fe	Mg	Ti	Zn
89,64	8,5	1,1	0,05	0,5	0,11	0,1

During calculations it was assumed that the material is isotropic and exhibits the features of an elastic – plastic body, introducing to calculations the, listed in a table, values of the stress-strain curve (nonlinear characteristics) obtained in the tensile tests conducted on a MTS testing machine (10T). Averaged results of static tensile tests carried out on φ = 8 mm diameter specimens are compared in Table 2. At this stage of material description, the invariability of material constants was assumed respective of the temperature and strain rate, adopting the Huber - Mises - Hencky condition of plasticity (HMH).

$$\sigma_0 = \frac{1}{\sqrt{2}}\left[(\sigma_1-\sigma_2)^2+(\sigma_2-\sigma_3)^2+(\sigma_3-\sigma_1)^2\right]^{\frac{1}{2}} \quad (1)$$

where:
σ_o – the yield stress

Table 2.
Mechanical properties of Al – Si alloy

$R_{0,2}$	R_m	A_5	Z	E	υ
[MPa]	[MPa]	[%]	[%]	[MPa]	
282.0	335.0	4,6	6.6	70120	0.33

The choice of the right constitutive model of the examined material is a key issue in solving the dynamic problems based on finite element method. Typically, two types of material models are used; the first is based on a law of plastic flow, the second takes into account the decohesion of material. Practical use of the majority of proposed models requires the experimental determination of constants in equations describing the phenomena of plastic deformation and destruction of material, hence the selected models are often a bit simplistic, although contain a description of the phenomena occurring during high-speed deformation. Johnson - Cook model is usually sufficiently accurate for modelling penetration phenomena in an object of high initial speed. This model is used in solving the problems of linear thermoelasticity, plasticity, plastic flow, isotropic consolidation, the effects associated with changes in strain rate, adiabatic thermal effects and material damage. According to Johnson - Cook law, the reduced stress is expressed by equation [6]:

$$\sigma_0 = \left[A + B\left(\varepsilon_{\text{int}}^{pl}\right)^n\right] \cdot \left[1 + C \cdot \ln\left(\frac{\varepsilon_{\text{int}}^{vpl}}{\varepsilon_0^v}\right)\right]\left(1 - T^m\right) \tag{2}$$

where:
A, B, C, n, m – the material variables,
ε_{int}^{pl} – the intensity of plastic strain,
ε_{int}^{vpl} – the equivalent plastic strain rate,
ε_o^v – the reference plastic strain rate,
T_T – the dimensionless temperature

$$T_T = \frac{T - T_0}{T_s - T} \tag{3}$$

where:
T – the instantaneous value of temperature,
T_s – the melting temperature,
T_0 – the ambient temperature.

During calculations, the instantaneous values of the intensity of plastic deformation at points of the integration of components are determined. It is understood that decohesion occurs when the damage parameter D is equal to unity. This damage parameter is defined by the following equation:

$$D = \sum\left(\frac{\Delta\varepsilon_{\text{int}}^{pl}}{\varepsilon_f^{pl}}\right) \tag{4}$$

where:
$\Delta\varepsilon_{int}^{pl}$ – the increment in the plastic strain intensity,
ε_f^{pl} - the critical value of the plastic strain intensity

Summing up in formula (4) takes place after each increment in deformation.

The critical value of the plastic strain intensity ε_f^{pl} depends on the dimensionless strain rate $\varepsilon_{int}^{vpl} / \varepsilon_o^v$ and on the average stress σ_m to stress intensity σ_{int} ratio. The average stress value is an arithmetic mean of normal stress components σ_1, σ_2, σ_3, while stress intensity is determined by HMH hypothesis. The value of ε_f^{pl} is determined by the following relation:

$$\varepsilon_f^{pl} = \left[D_1 + D_2 \exp\left(D_3 \frac{\sigma_m}{\sigma_{\text{int}}}\right)\right] \cdot \left[1 + D_4 \ln\left(\frac{\varepsilon_{\text{int}}^{vpl}}{\varepsilon_0^v}\right)\right] \cdot \left(1 + D_5 T_T\right) \tag{5}$$

where:
$D_1 – D_5$ – the material constants determined experimentally.

If the failure criterion is met, the σ_m / σ_{int} quotient takes the zero value and keeps this value throughout the whole further analysis. This means that, starting with that moment, the damaged component does not carry the loads any longer and is removed from the whole structure. Phenomenological equation (5) consists of three members related with stress, strain rate and temperature, for which the constant values D are determined in mechanical tests. Constants D_1, D_2 and D_3 were determined experimentally during the tensile test carried out on tensile specimens with annular notch of variable radius, while other values were adopted from Bovril's work [7].

3. Material testing

Mechanical tests to determine the constants D_1 , D_2 and D_3 were carried out in a tensile test using a φ = 14 mm specimen (Fig. 1) with an annular notch of φ = 1.0, 1.5, 2.0, 3.0, 4.0 and 7.0 mm.

The distribution of stresses within the area of the annular notch made in a rod can be determined by Bridgman's solution [8]. This solution interrelates the degree of the triaxiality of the state of stress T_t, in middle part of the specimen with the geometry of the specimen in which the annular notch was made using the following relationship:

$$T_t = \frac{\sigma_m}{\sigma_{\text{int}}} = \frac{1}{3} + \ln\left(1 + \frac{R}{2\rho}\right) \tag{6}$$

where:
σ_m – the average stress value is an arithmetic mean of the normal stress components σ_1, σ_2, σ_3:

$$\sigma_m = \frac{\sigma_1 + \sigma_2 + \sigma_3}{3} \tag{7}$$

where:
σ_{int} – the stress intensity determined by HMH hypothesis:

$$\sigma_{\text{int}} = \frac{1}{\sqrt{2}}\left[\left(\sigma_1 - \sigma_2\right)^2 + \left(\sigma_2 - \sigma_3\right)^2 + \left(\sigma_3 - \sigma_1\right)^2\right]^{\frac{1}{2}} \tag{8}$$

The degree of the triaxiality of the state of stress T_t affects the process of cracking of the plastic material because the spherical stress tensor component σ_m is associated with the process of the initiation and growth of voids [9], [10], [11]. The annular notch causes a significant decrease in the value of the deformation compared with a smooth sample, while an increase is observed in the force at which the rupture of the specimen occurs (Fig. 2).

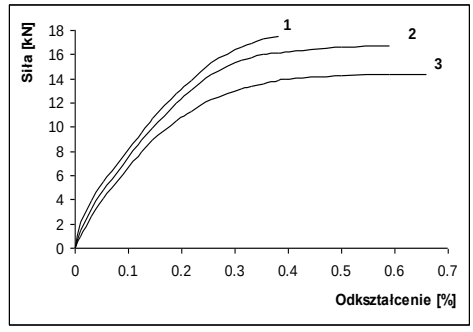

Fig. 2. Tensile curves plotted for specimens with annular notches of 1- φ = 2 mm, 2 – φ = 4 mm, 3 – φ = 7 mm
Siła – force, Odkształcenie – strain

The alloy decohesion mode also changes. The scanning photograph of the centrally formed fracture in an unnotched specimen shows visible areas of plastic deformation (Fig. 3d). An incision made in the annular notch increases the share of brittle fracture. the more that the annular notch has a small radius (Fig.3). When the radius φ is 2mm (Fig. 3a), the fracture shows no longer the presence of the zones of plastic deformation in its central part. These differences in the type of material decohesion are caused by changes in the state of stress and strain in the notch plane under the influence of increasing load. assumimg different run when the radius of the annular notch changes. The effect of the spatial state of stress on decohesion mode in the Al - Si alloy under consideration was discussed in detail in the author's study [12]

Table 3.
The triaxiality degree T_t and the related maximum strain ε_{max} for Al –Si alloy

φ [mm]	ε_{max}^{*}	T_t^{**}
1.0	0.006	1.34
1.5	0.02	1.11
2.0	0.022	0.96
3.0	0.026	0.79
4.0	0.037	0.69
7.0	0.045	0.55
0.0	0.046	0.33

* - experimental values
** - numerical values

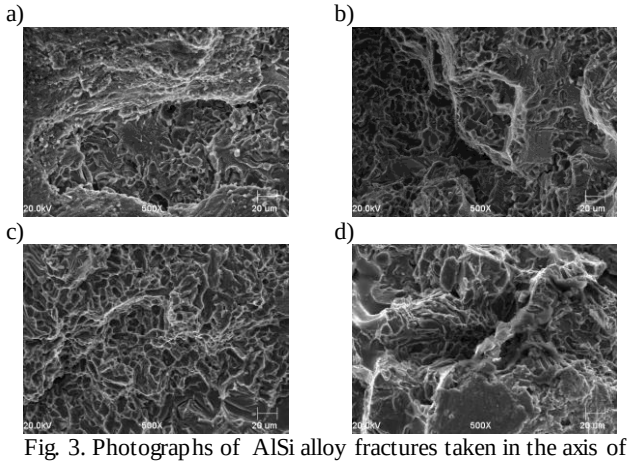

Fig. 3. Photographs of AlSi alloy fractures taken in the axis of specimens with annular notches of different radii φ: a - φ = 2 mm, b - φ = 4 mm, c - φ = 7 mm d – unnotched specimen; 500x

It was assumed that the penetrator is made of cast steel. the mechanical properties of which, experimentally determined on cylindrical φ = 8 mm specimens, are summarised in Table 4.

Table 4.
Mechanical properties of cast steel

$R_{0,2}$	R_m	A_5	Z	E	υ
[MPa]	[MPa]	[%]	[%]	[MPa]	
564.0	696.5	24,5	30,5	190000	0.33

A non-linear elastic - plastic model, similar to that functioning in Al - Si alloys, was adopted, allowing for a relationship between the alloy effort, the degree of stress triaxiality, true strain on decohesion, and plastic strain rate (Table 5).

Table 5.
Triaxiality degree T_t and maximum strain ε_{max} for cast steel

φ [mm]	ε_{max}^{*}	T_t^{**}
1.0	0.05	1.1
0.0	0.245	0.33

* - experimental values
** - numerical values

Johnson - Cook model implemented in Abaqus programme requires additionally the determination of a critical value of the internal energy in a unit model volume E_{IK}.

The critical value of internal energy E_{IK} was determined by experiments during compression tests carried out on casting of a trapezoidal structure, recording force as a function of changes in the original height. The compression graph for structures of this type has a characteristic shape described in the reference literature [13]. Based on the experimentally determined set of curves, the total value of internal energy E_{IK} = 232 J was calculated; it corresponds to the surface area under the curve ranging from zero up to the value obtained at an instant of the structure compaction (Fig. 4). A unit value of this energy falling to 1 mm^3 of the structure is 8.1 J.

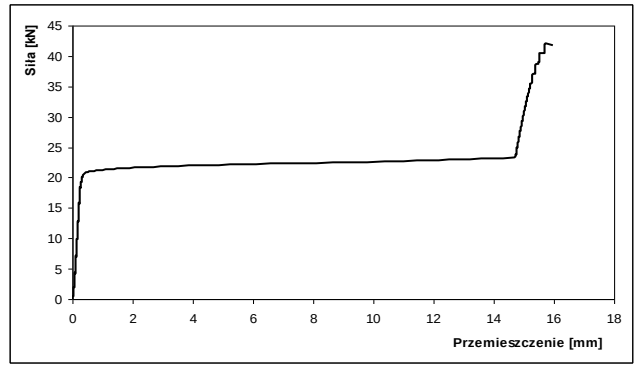

Fig. 4. Compression curve for trapezoidal cellular structures

3.1. Boundary and initial conditions

Table 6.
Mass and density compared for cellular structure and Al – Si alloy

	Mass	Volume	Density	Relative density
	[g]	[mm^3]	[g/mm^3]	Δ**
Cellular structure	77	28507	0,001175	0,4352
Al-Si alloy	177*	65548	0,002700	-

* - mass of cuboid of overall dimensions corresponding to the dimensions of cellular structure
****** - relative density of cellular structure Δ defined as a ratio between the density of porous material and the starting material ρ_s

4. Results

The performed numerical calculations aimed at the determination of changes in penetrator velocity during structure perforation and at the determination of the dissipation energy. Owing to the structure configuration, during its perforation, there is a difference between the penetrator tip and end speed. Characteristic is the initial drop in the penetrator tip speed from V_p = 700 m/s to 180 m/s caused by the erosion and flattening during impact contact with the top surface. On piercing the top layer, the penetrator energy decreases but the decrease is not strong enough to prevent the recurrent increase when the penetrator enters a void area in the structure. Farther elements of the structure slowdown the penetrator movement. The penetrator end, which does not undergo deformation, reduces its speed only slightly at the beginning to make it equal with the speed of the tip after piercing of the structure. Ultimately, the penetrator pierces and leaves the structure at a speed of V_k of 395 m/s.

Table 7.
Changes in energy ΔE and velocity ΔV upon perforation of the structure

V_p	V_k	V_p- V_k	t_{pr}*	E_p**	E_k	E_p- E_k
[m/s]	[m/s]	[m/s]	[ms]	[J]	[J]	[J]
715	395	320	0,046	1990	695	1295

* - t_{pr} – penetration time counted until structure perforation by the penetrator tip
** - E_p –penetrator starting energy,
*** - E_k –penetrator end energy

Figures 5 and 6 show stress values obtained by numerical analysis according to the HMH hypothesis in the following time sequences of structure perforation with the penetrator.

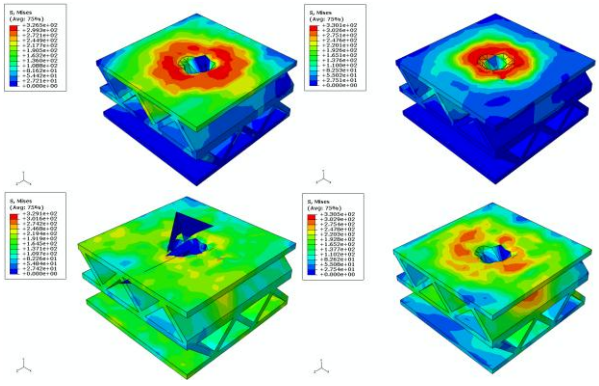

Fig. 5. HMH stresses in structure during perforation with penetrator; time 1 – 0,00001 s, 2 – 0,00002 s, 3 – 0,00003 s, 4 – 0,00010 s

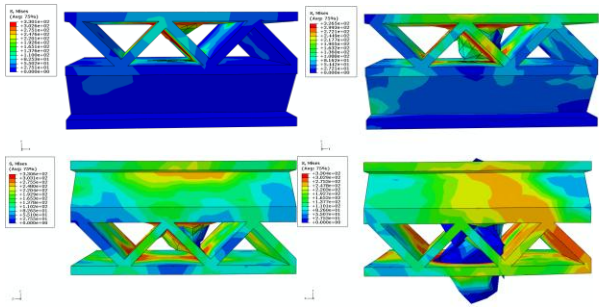

Fig. 6. HMH stresses in structure during perforation with penetrator; time 1 – 0,00001 s, 2 – 0,00002 s, 3 – 0,00004 s, 4 – 0,00007 s

Table 8.
The results of MES calculations: the starting and end velocity and the depth of penetration

V_p	V_k	V_p- V_k	d_{pr}*	t_{pr}**
[m/s]	[m/s]	[m/s]	[mm]	[ms]
715	675	40	25,4	0.0375
500	472	28	25,4	0,051
400	375	25	25,4	0,0625
200	125	75	25,4	0,152
100	0	100	16,42	0,325
50	0	50	6,08	0,2125
25	0	25	3,41	0,175

Acknowledgements

Scientific researches financed from development project No. OR00009012.

References

[1] S. McKown: The quasi-static and blast loading response of lattice structures, International Journal of Impact Engineeannular, Vol. 35, pp. 795 – 810, 2008
[2] W. Hou, F. Zhu: Ballistic impact expariments of metallic sandwich panels with aluminium foam core, International Journal of Impact Engineeannular, Vol. 37, pp. 1045 – 1055, 2010
[3] Dean J.: Energy absorption duannular projectile perforation of thin steel plates and kinetic energy of ejected fragments, International Journal of Impact Engineeannular, pp. 1 - 9, 2009
[4] Włodarczyk E.: Hydrodynamiczne modele wnikania długiego pręta w tarczę, Materiały z III Konferencji Naukowo-Technicznej, "Odporność Udarowa Konstrukcji", 2001, s. 285 - 316
[5] Piekło J., Pysz S., Małysza M: Proces wykonania i mechaniczne właściwości odlewanych, uporządkowanych konstrukcji komórkowych ze stopu Al.-Si, Prace Instytutu Odlewnictwa Tom L, Nr 4, Kraków 2010

[6] Gupta N.K., Iqubal M.A., Sekhon G.S.: Experimental and numerical studies on the behavior of thin aluminium plates subjected to impact by blunt and hemispherical-nosed projectiles, International Journal of Impact Engineeannular, Vol. 32, pp 1921-1944, 2006
[7] Borvik T., Clausen H., Hopperstad S., Benallal A.: Flow and fracture of aluminium alloy AA5083-H116 as function of strain rate, temperature and triaxiality, Materials Science and Engineeannular, A364, pp. 260-272, 2004
[8] Gołaski L.: Elementy doświadczalnej mechaniki pękania, Politechnika Świętokrzyska, Kielce 1992
[9] Teirlinck D., Zok F., Embury J., Ashby M.: Fracture Mechanism Maps in Stress Space, Acta Metallurgica, Vol.36, No. 5, 1988, pp. 1213-1228
[10] Argon S., Im J., Safoglu R.: Cavity Formation from Inclusions in Ductile Fracture, Metallurgical Transactions, Vol. 6A, 1975, pp. 825-837
[11] Kown D., Asaro R.: A Study of Void Nucleation, Growth and Coalescence in Spheroidized 1518 Steel, Metallurgical Transactions, Vol. 21A, 1990, pp. 117-134
[12] Piekło J., Maj M.: Effect of annular notch radius on the decohesion mode In AlSi alloys, Archives of Foundry Engineeannular, Vol. 9, Issue 2, April – June 2009 s. 25 – 28.
[13] Gibson L. J., Ashby M. F.:Cellular Solids – Structure and Properties, Pergamon Press, Oxford – Toronto, .